Journal of Magnetism and Magnetic Materials 427 (2017) 156–161

Contents lists available at ScienceDirect

Journal of Magnetism and Magnetic Materials

journal homepage: www.elsevier.com/locate/jmmm

Dual-frequency magnetic particle imaging of the Brownian particle contribution

Thilo Viereck*, Christian Kuhlmann, Sebastian Draack, Meinhard Schilling, Frank Ludwig

Institut für Elektrische Messtechnik und Grundlagen der Elektrotechnik, TU Braunschweig, Braunschweig, Germany

ARTICLE INFO

Keywords:
Magnetic particle imaging
Magnetic nanoparticles
Brownian and Néel relaxation

ABSTRACT

Magnetic particle imaging (MPI) is an emerging medical imaging modality based on the non-linear response of magnetic nanoparticles to an exciting magnetic field. MPI has been recognized as a fast imaging technique with high spatial resolution in the mm range. For some applications of MPI, especially in the field of functional imaging, the determination of the particle mobility (Brownian rotation) is of great interest, as it enables binding detection in MPI. It also enables quantitative imaging in the presence of Brownian-dominated particles, which is otherwise implausible. Discrimination of different particle responses in MPI is possible via the joint reconstruction approach. In this contribution, we propose a dual-frequency acquisition scheme to enhance sensitivity and contrast in the detection of different particle mobilities compared to a standard single-frequency MPI protocol. The method takes advantage of the fact, that the magnetization response of the tracer is strongly frequency-dependent, i.e. for low excitation frequencies a stronger Brownian contribution is observed.

1. Introduction

Magnetic nanoparticles with core diameters of around 25 nm, which are favorable for MPI [1], can relax both via the Néel mechanism and the Brownian rotational motion, which makes it possible to discriminate the particle binding state or the viscosity of the medium. With that, MPI is promoted to a functional imaging method, where functionalized nanoparticles can be selectively imaged. We demonstrate that we can provide the spatial distribution of the particles in the imaging plane and at the same time estimate the particle mobility, equivalent to the Brownian time constant depending on hydrodynamic volume and/or the viscosity of the medium. Most MPI scanners work with sinusoidal excitation fields in the frequency range around 25 kHz, where a Néel-dominated response is observed for most tracers. As such, MPI is not particularly sensitive to characteristic Brownian frequencies in the lower kHz range, typically found in physiological media. Therefore, the imaging sequence of the scanner has to be modified and adjusted for maximized sensitivity towards binding detection. In this contribution, we introduce a new approach to achieve sensitive binding detection in MPI. For that, the standard MPI imaging protocol at 25 kHz is advanced into a dual-frequency approach operating at 25 kHz and 10 kHz. The method takes advantage of the frequency-dependence of the particle's magnetization response to discern particles with different Brownian time constants [2].

2. Materials and methods

2.1. Particles

For the experiments, we employ FeraSpin™ XL from nanoPET Pharma GmbH (Berlin, Germany). FeraSpin™ R is a multi-core particle system with a crystallite size of about 6–7 nm and an average hydrodynamic diameter of about 65 nm. The dynamic magnetic properties of FeraSpin™ R have been studied before [3]. The majority of particles in FeraSpin™ relaxes via the internal Néel mechanism (baseline contribution). In order to study the mobility of particles (=binding state or viscosity of the medium), it is essential for the particles to at least partially relax via the Brownian rotational mechanism. FeraSpin™ XL from the FeraSpin™ series is a size-selected portion of the original FeraSpin™ R, which was found to exhibit a maximum of Brownian contribution within the FeraSpin™ particle family in magnetic particle spectroscopy (MPS) measurements [4,5].

The Brownian rotational motion is described by the Brownian relaxation time $\tau_B = 3\eta V_h/k_B T$ with the viscosity η of the medium, the hydrodynamic diameter V_h, Boltzmann constant k_B and temperature T. The characteristic relaxation time for a given particle type can be determined experimentally by means of ac susceptibility (ACS) measurements (Fig. 1). For FeraSpin™ XL, the equivalent characteristic frequency $\omega = 1/\tau_B$ is found to be approximately $f = \omega/2\pi = 1.7$ kHz

* Corresponding author.
E-mail address: t.viereck@tu-bs.de (T. Viereck).

http://dx.doi.org/10.1016/j.jmmm.2016.11.003
Received 27 June 2016; Received in revised form 21 October 2016; Accepted 1 November 2016
Available online 04 November 2016

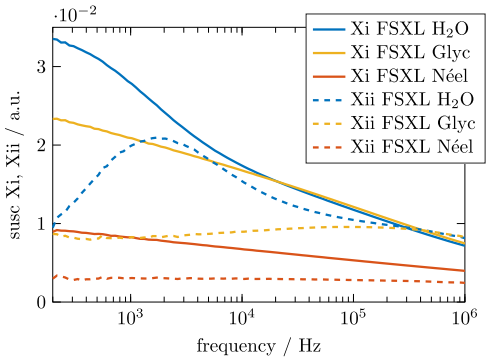

Fig. 1. AC susceptibility spectra of aqueous suspension, water-glycerol solution and freeze-dried FeraSpin™ XL sample. Imaginary part of aqueous suspension shows a pronounced Brownian contribution around (and below) 1.7 kHz.

(from maximum of the imaginary part Xii in Fig. 1).

Generally, the relaxation times are strongly field-dependent [6,7]. For a large ac amplitude (in the range of several mT), as it is employed for magnetic particle spectroscopy (MPS) and magnetic particle imaging (MPI), the actual Brownian relaxation time is expected to be higher than obtained from ACS. The modified Brownian time constant $\tau_B(\xi) = 3\eta V_h/\sqrt{1 + 0.07\xi^2}k_BT$ with $\xi = \mu_0 mH/k_BT$ was approximated by Yoshida et al. [8] (from Fokker-Planck simulations). From Fig. 1 it becomes clear, that at a drive field frequency of 10 kHz (or 25 kHz respectively), there is still a pronounced Brownian contribution (Fig. 1, H_2O) of the particles evident compared to the Néel background (Fig. 1, Néel). At the low frequency end of the ac susceptibility spectrum (200 Hz), an amplitude ratio of 1: 1 for Néel: Viscous/glycerol and 1:2 for Néel:H_2O is determined. It shows that for different viscosities the choice of excitation frequency is more critical than for basic Néel/Brownian discrimination, especially because a certain portion of the size distribution contributes a secondary peak in the imaginary ACS part above 100 kHz. The observation of a significant Brownian contribution is confirmed from MPS measurements on the same sample at the relevant drive field frequencies and with a nominal ac amplitude of 25 mT (Fig. 2). Magnetic particle spectroscopy (MPS) exploits the non-linearity of the dynamic magnetization curve similar to an MPI system and therefore provides an MPI-relevant characterization of the MNP tracer response [4].

For an immobilized sample (Fig. 2, Néel), only a small frequency dependence of the magnetization response is observed. In contrast, the mobile (Fig. 2, H_2O) and viscous (Fig. 2 Glyc, particles suspension +glycerol) samples show a different response for both excitation frequencies, i.e. the slope of harmonic decay is steeper for 25 kHz. The distinction between samples with different viscosity (and therefore particle mobility) is also frequency-dependent. For 10 kHz a good distinction between the mobile and viscous samples is observed (Fig. 2,

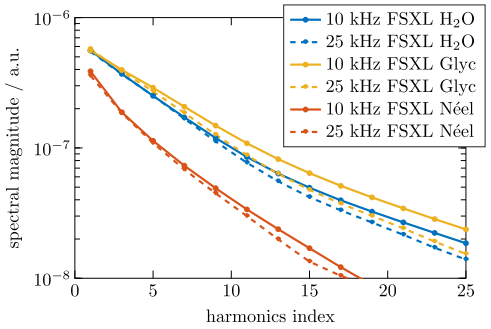

Fig. 2. Magnetic particle spectroscopy (MPS) spectra of FeraSpin™ XL in DI water, water-glycerol mixture and freeze-dried measured at excitation frequencies of 10 kHz and 25 kHz (amplitude of 25 mT). A prominent Brownian contribution is evident in the H_2O and viscous (glycerol) samples.

10 kHz H_2O and Glyc), whereas for 25 kHz the difference in MPS response magnitude is approximately 2-times smaller (Fig. 2, 25 kHz H_2O and Glyc). Also, the differences are larger at higher harmonic indices (1.86x at the 5th harmonic and 2.50x at the 15th harmonic), so that the mobility contrast improves with availability of more higher harmonics (above an SNR threshold) in an imaging experiment. The variation of the magnetization responses at different frequency provides the motivation for the proposed dual-frequency MPI design.

2.2. Scanner hardware/acquisition scheme

The experiments were performed utilizing a newly developed dual-frequency MPI scanner. Based on the design of our previous scanner [9,10], new 2D FFP (field-free point) imaging hardware was constructed to support drive fields of around 10 kHz and 25 kHz. The lower 10 kHz frequency was chosen to maximize the Brownian contribution from the tracer while keeping a reasonable SNR margin (receive signal degrades towards lower frequencies due to induction law) to detect diluted particle samples (and viscosity series). The scanner was operated in 1D mode, with a single transmit coil (along the x direction of the instrument) at 30 mT excitation amplitude and two orthogonal receive coils (collinear in x-direction and perpendicular in y-direction to the transmit axis). In presence of a 1 T/m imaging gradient of the selection field, the 1-dimensional field-of-view (FOV) of the experiment is about 40 mm in length. The standard acquisition parameters for the instrument enfold an analogue receive bandwidth of 1 MHz and a 500 ms (10 kHz) resp. 320 ms (25 kHz) measurement/acquisition time per frame (with 10-fold averaging). For the imaging experiments, the particles were filled into acrylic cuboids with a dash contour (4 mm long, 1.5 mm wide and 1.5–3.0 mm deep). A line scan orthogonally to the dash line shows a point-sample in the 1D FOV. The particle in the remaining dimensions of the line help to improve the SNR of the experiment.

2.3. Reconstruction

An analysis of the system matrix components at both frequencies (Fig. 3) for a selected point in the FOV reveals only marginal differences of the response magnitude (Fig. 3, left) [11]. As expected from linear Debye theory (cf. ACS in Fig. 1), a change of $\omega\tau$ by magnetization dynamics (time constant τ) or sampling frequency ω is associated with a phase shift/deviation that is most prominent around $\omega\tau = 1$. While the magnitude stays nearly constant, the real part of the magnetization response reveals a strong effect on encoded phase for different excitation frequencies (Fig. 3, right).

Although the Debye model does not strictly apply for large excitation amplitudes into the non-linear range of the magnetization curve, it readily predicts a phase shift as observed in the data. When the Néel baseline contribution (which is not sensitive to particle mobility) is treated correctly, a Debye-based model [12] might therefore give an adequate description for a calibration-less approach (for a variety of different mobility states, i.e. different viscosities). In such an approach, the mobility-related change in magnetization response could be modeled numerically, while only few calibration points (including the Néel reference) are determined experimentally.

In Fig. 4, the real part (Fig. 4, upper row) and imaginary part (Fig. 4, lower row) of the complex-valued spectral signature is displayed as a difference of the 10 kHz response minus the 25 kHz response for a selected point in the FOV. It can be seen, that for H_2O ($\eta \approx 1$ mPas) the difference between the two frequencies in spectral amplitude is smaller than for a viscous sample (Glyc, $\eta \approx 180$ mPas). Also, the differences for the H_2O sample are limited to the lower harmonics compared to the glycerol sample. The overall larger differences for the viscous sample are due to the fact that for slow relaxing particles (long Brownian time constant from a high viscosity of the medium) the 25 kHz signal is comparable, but the 10 kHz

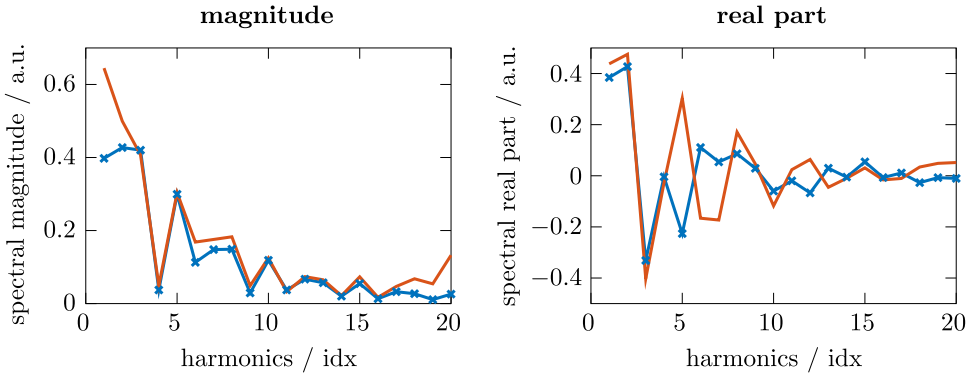

Fig. 3. Comparison of spectral signatures at a selected point in the FOV between 10 kHz (blue) and 25 kHz (orange). While the magnitude (left) shows only small variations on frequency, the real part (right) depicts a distinct shift, which translates mostly into a phase variation. (For interpretation of the references to color in this figure legend, the reader is referred to the web version of this article.)

measurement still reveals an additional (Brownian) contribution.

In order to establish a reconstruction scheme for dual-frequency MPI, a joint reconstruction approach as suggested by Rahmer et al. [13] is considered. The system matrix is constructed to actually comprise multiple distinct system matrices for the different particle contributions. In case of "multi-color" MPI, calibrations for the different particle "types" are combined. The same idea can easily be transferred to the case where we calibrate for different particle mobilities. However, the calibration matrices for different viscosities are much less distinct.

For that reason, the system matrix for joint reconstruction, is extended to cover two different drive field frequencies. From Debye theory and confirmed by MPS measurements (Fig. 2), we know that this provides an additional degree of freedom on the data, because of the frequency-dependence of the magnetization response, which varies for different mobility states. Thus, we construct a composite system matrix that incorporates two different viscosities and the two different drive field frequencies in a 2×2 matrix (each sub-matrix contains both receive channels), i.e. the composite matrix is composed of four complete/standard system matrices for the individual parameter combinations. The resulting system matrix is compatible with the "multi-color" MPI reconstruction approach [13], i.e. joint reconstruction, but with augmented frequency components. The composite matrix is schematically drawn in Fig. 5. For the stated experiment, the following composition of the matrix is used: f_1=10 kHz, f_2=25 kHz and η_1=H_2O, η_2=Néel.

Since, due to the induction law, the receive amplitudes of the 25 kHz system are larger than for the 10 kHz design, the system matrix components are scaled by 2.5 accordingly. A graphical representation (surface plot) of the composite system matrix of the dual-frequency experiment is shown in Fig. 6a and a grayscale view in Fig. 6b.

At 25 kHz an almost identical response from the mobile H_2O (Fig. 6a, right back) and the immobile Néel (Fig. 6a, left back) samples are observed, but at 10 kHz the additional Brownian contribution

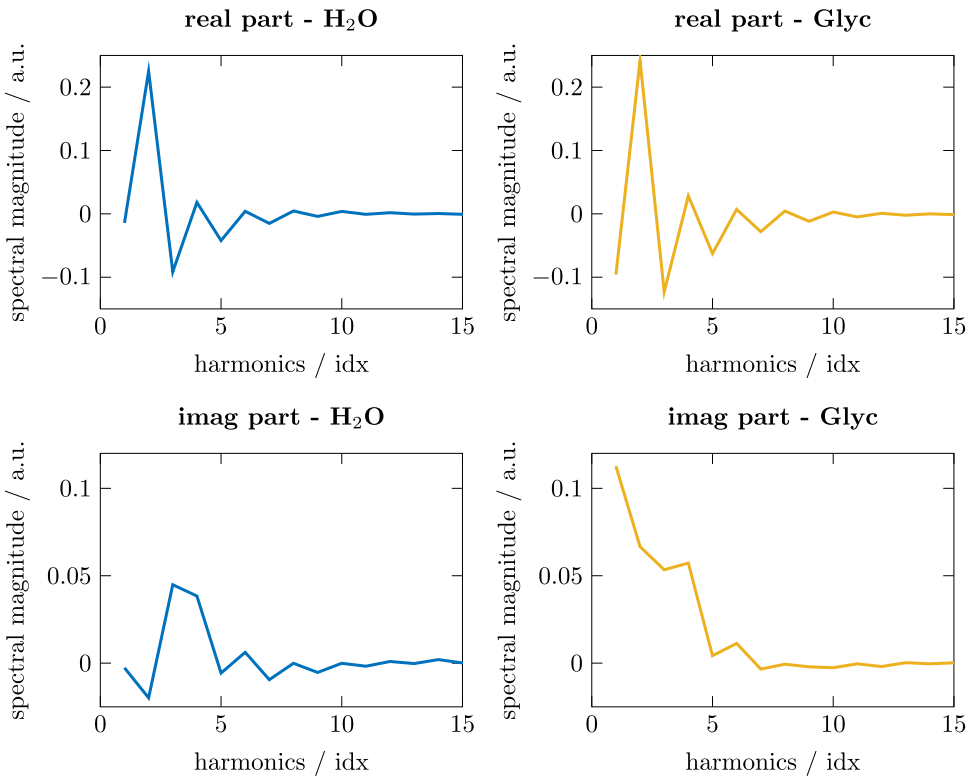

Fig. 4. Difference responses (10–25 kHz) at a selected point in the FOV (same as in Fig. 3) for the real part (upper row) and imaginary part (bottom row) of the complex-valued magnetization response.

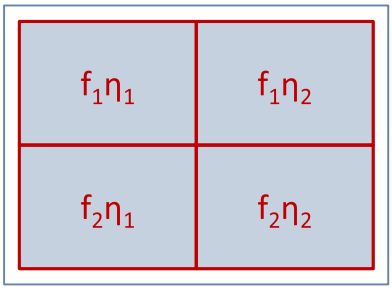

Fig. 5. Composite system matrix for joint reconstruction of two different viscosities (η_1 and η_2) is augmented vertically for dual-frequency MPI (f_1 and f_2).

(assumed from MPS data, Fig. 2) delivers a much stronger magnitude for the H_2O sample (Fig. 6a, right front). For the characteristic Brownian frequency shifting to higher frequencies at large excitation amplitudes, the 10 kHz signal is evidently close enough to create a strong Brownian response for FeraSpin™ XL particles. The large signal Brownian time constant with sinusoidal excitation is approximated from $\tau_B(\xi)$ to around 5.6 kHz ($\xi \approx 12$). The same observation is made in Fig. 6b, where the magnitude of the composite system matrix is shown as a grayscale image.

3. Results and discussion

Initial results of the dual-frequency MPI using a composite system matrix in a joint reconstruction are shown in comparison with single-frequency MPI images. For all reconstructed images in this section the iterative Kaczmarz algorithm (or algebraic reconstruction technique) is employed. For comparison, the same number of harmonics are included for 10 kHz and 25 kHz in Fig. 7 to ensure comparable conditions. Generally (in the present system), for 10 kHz a higher number of harmonics is available, and they are included for the final results in Fig. 9 ff., but omitted here to allow for a fair comparison. Reconstruction results from joint reconstruction with η_1 and η_2 are shown in Fig. 7. Here, the reconstruction from a single frequency at 10 kHz and 25 kHz are shown (Fig. 7, first two rows) in comparison with results from the dual-frequency acquisition (Fig. 7, both).

To demonstrate and discuss the stability of the regularized solution, the results are shown for identical data and system matrices but with different levels of regularization. The reconstruction parameter is not optimized for the individual image, i.e. no treatment of different SNR/weighting, so that the strong effect of regularization on the images becomes obvious. For all scenarios a successful reconstructed image is recognized. Image quality (sharpness, artifacts, ...) and contrast differ, though. The phantom is constructed from two dashes (H_2O left, viscous/glycerol right) with identical concentration, which should be visible as two confined bands (with identical intensity) in the images. For 10 kHz (Fig. 7, top row), the two band are clearly reproduced (even with little regularization). The 25 kHz data, on the other hand, also shows two band, but it produces more artifacts and needs stronger regularization in order to provide good results. The combined approach (Fig. 7, bottom row) shows again distinct results and from visual inspection could be classified as a blend of 10 kHz and 25 kHz data. From these findings, it can be assumed that the inclusion of both frequencies in the composite system matrix improves the conditioning of the system matrix and therefore requires less regularization. The claim is supported by the condition numbers of the respective system matrices (given separate with respect to the η channels) in Table 1.

The condition number of the dual-frequency system matrix is greatly reduced compared to using only a single drive field frequency. Also, a higher and narrower PSF (e.g. 10 kHz H_2O) seems beneficial for reconstruction.

The properties (contrast, definition, etc.) of the reconstructed images (Fig. 7) are better seen from the corresponding profiles in Fig. 8. As expected from Fig. 6, at 25 kHz both samples (with different mobility) give almost the same results. The estimated concentration is about the same for both samples, only the width of the right band is a little broader, corresponding to the limited mobility of the viscous sample. For 10 kHz, the observations are basically the same, only that the H_2O sample (Fig. 8, left) shows a much higher intensity, which means that the concentration has been overestimated compared to the viscous sample (Fig. 8, right). In direct comparison, the point-spread function (PSF) of the 25 kHz data is broader than for 10 kHz, i.e. blurring from relaxation plays potentially a greater role. The PSF of the dual-frequency data appears to be limited from 25 kHz as well (PSF width between 10 kHz and 25 kHz).

Without further adjustments, the dual-frequency approach delivers the best contrast (maximum intensity to background ratio), while the 25 kHz contrast is last (smaller Brownian contribution leads to smaller frequency-normalized SNR in the present system). Quantification of the particle concentration varies greatly between the frequencies. Ideally, the intensity ratio of the two dashes (with identical concentration) should be 1. From Fig. 8 the actual ratios (average over central FOV region) are determined as 0.96 for 25 kHz, 1.63 for 10 kHz and 1.43 for dual-frequency. For the given imaging parameters and the given particle system 25 kHz is almost quantitative.

The following images demonstrate the dual-frequency “Mobility MPI” (mMPI) approach with optimized imaging and regularization parameters. In Fig. 9 mobile and immobile contributions are discriminable with a high degree of separation between the individual mobility channels (η_1 and η_1).

The sharper PSF for the mobile part enables a higher resolution.

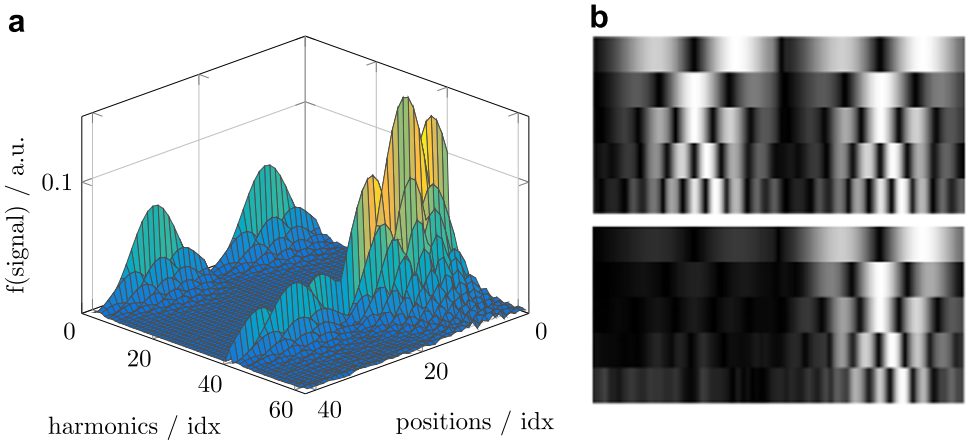

Fig. 6. a) Surface representation of the composite system matrix (dimensions flipped with respect to Fig. 5). Harmonic indices 1–39 are the 25 kHz channels, 40–63 show the 10 kHz components. Mobile sample (H_2O) shown right to the immobile (Néel) sample (on the left). **b)** Grayscale-encoded magnitude representation of the composite system matrix (cf. Fig. 5).

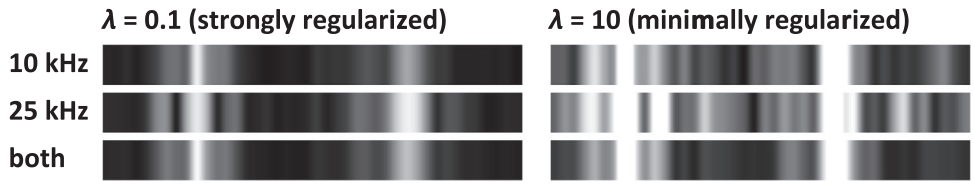

Fig. 7. Comparison of joint reconstruction results for data acquired at 10 kHz (first row), 25 kHz (second row) and using the system matrix with both frequencies (third row). Results are shown for two levels of regularization, a minimally regularized solution (right column) and with strong regularization (left column). Ideally, two narrow bands (δ-sample) should be visible from the H_2O (left) and Glyc (right) samples.

Table 1
Condition numbers of composite system matrices.

	10 kHz	25 kHz	Both
η_1 (H_2O)	776	3600	266
η_2 (Néel)	2700	3200	763

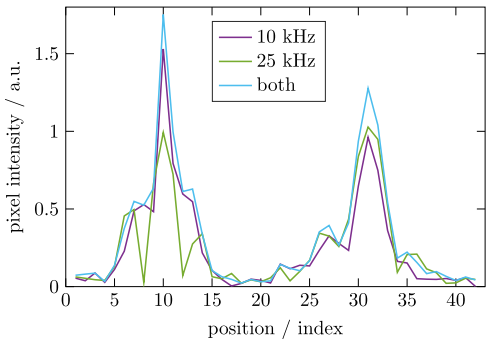

Fig. 8. Line profiles from Fig. 7 show contrast proportions of the images, mobile (left, index 10) and viscous/immobile sample (right, index 31).

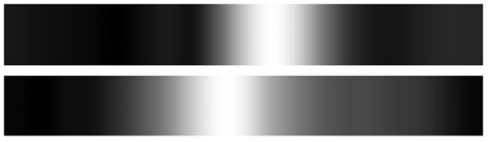

Fig. 9. Phantom image of two adjacent lines/dashes, one filled with a FeraSpin™ XL suspension (η_1, top) and the other with the same particles immobilized in a Mannitol-D matrix (η_2, bottom).

This is better observed in Fig. 10, where line scans for particles in all possible position in the 1D FOV (mechanically moved by the calibration robot) are adjoined into a 2-dimensional representation. The mobile part (Fig. 10, left) displays a confined diagonal, while the immobile part (Fig. 10, center) is significantly broadened (due to limited particle mobility). In the false color overlay (Fig. 10, right), the two separate channels are superimposed to show the mobile part (yellow) and the immobile part (blue). The spatial separation of the dashes reveals a limited resolution as result of the weak imaging gradient of 1 T/m, still the mobility channels are clearly discernable.

4. Conclusion

The dual-frequency approach for the discrimination of different particle mobilities in MPI seems promising. A single frequency in combination with a joint reconstruction approach, as suggested for "multi-color" MPI, can be used to estimate and distinguish different particle mobility (and not just different particle type with discernable spectra). However, the image contrast (and potentially sensitivity for small mobility variations) can be enhanced by addition of a second drive field frequency. Based on the above data, contrast improvements in the range of 14–32% were observed compared to a single-frequency acquisition scheme (here mainly compared to 10 kHz). Obviously, a low drive field frequency is advantageous to capture a significant Brownian contribution and therefore enhance mobility estimation. The additional complexity in imaging hardware (due to a second drive field frequency) has to be considered.

For reconstruction, it was shown, that at 25 kHz a quantitative concentration is obtained, while at 10 kHz a strong (phase-)effect from the additional Brownian particle contribution is observed. Therefore, one might consider a different reconstruction strategy, or even mobility estimation as a post-processing step. Also, the introduction of temporal/spatial modulation could be helpful for improved binding/mobility contrast. The quantification of the concentration (and particle mobility) is critical for MPI and should be studied for different particle systems and in different media. The "Mobility MPI" approach provides a method to analyze and potentially correct for invalid concentrations.

Our preliminary data suggests that we can interpolate particle mobility from a limited set of calibration data (or viscosity channels in the system matrix) and that viscosity resolution degrades strongly towards higher viscosities (which is expected from [12]). However, the quantitativeness of the approach and translation to 2D MPI is considered for future work.

Acknowledgement

Financial support by the European Commission Framework Programme 7 under the NanoMag project (grant agreement no:

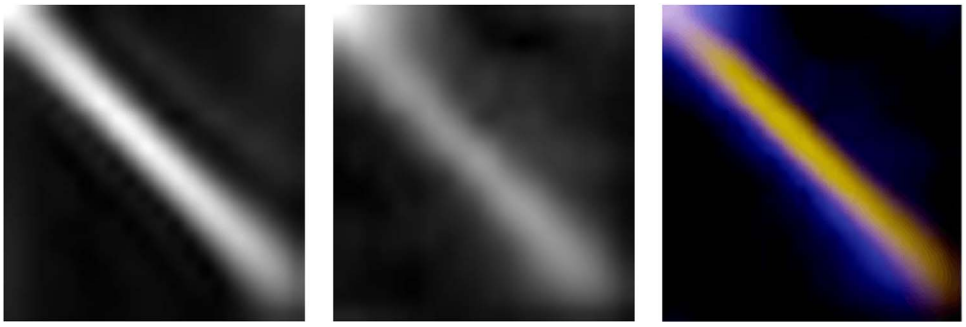

Fig. 10. Phantom with two adjacent lines/dashes, one filled with a FeraSpin™ XL suspension and the other with the same particles immobilized in a Mannitol-D matrix: reconstruction of the phantom in a 1D FOV at 1 T/m imaging gradient shows a good separation of the mobile (left) and immobile (center) parts. False color overlay of both contributions in the same image (right, blue=immobile, yellow=mobile). (For interpretation of the references to color in this figure legend, the reader is referred to the web version of this article.)

604448), by the German Research Foundation DFG (LU 800/5-1) and via SPP1681 (SCHI 383/2-1) is acknowledged. Thank you to nanoPET Pharma GmbH for providing us with FeraSpin™ XL particles for the experiments and H. Remmer for sample preparation and ACS measurements.

References

[1] B. Gleich, J. Weizenecker, Tomographic imaging using the nonlinear response of magnetic particles, Nature 435 (2005) 30.
[2] T. Wawrzik, F. Ludwig, M. Schilling, "Exploring particle mobility", in magnetic particle imaging, Springer Proc. Phys. 140 (2012) 21–25.
[3] D. Eberbeck, F. Wiekhorst, S. Wagner, L. Trahms, How the size distribution of magnetic nanoparticles determines their magnetic particle imaging performance, Appl. Phys. Lett. 98 (2011) 182502.
[4] S. Biederer, T. Knopp, T.F. Sattel, K. Luedtke-Buzug, B. Gleich, J. Weizenecker, J. Borgert, T.M. Buzug, Magnetization response spectroscopy of superparamagnetic nanoparticles for magnetic particle imaging, J. Phys. D: Appl. Phys. 42 (2009).
[5] F. Ludwig, T. Wawrzik, T. Yoshida, N. Gehrke, A. Briel, D. Eberbeck, M. Schilling, Optimization of magnetic nanoparticles for magnetic particle imaging, IEEE Trans. Magn. 48 (11) (2012).
[6] P.C. Fannin, S.W. Charles, C. Mac Oireachtaigh, S. Odenbach, Investigation of possible hysteresis effects arising from frequency- and field-dependent complex susceptibility measurements of magnetic fluids, J. Magn. Magn. Mater. 302 (2006) 1–6.
[7] F. Ludwig, A. Guillaume, M. Schilling, N. Frickel, A.M. Schmidt, Determination of core and hydrodynamic size distributions of $CoFe_2O_4$ nanoparticle suspensions using ac susceptibility measurements, J. Appl. Phys. 108 (2010) 033918.
[8] T. Yoshida, K. Enpuku, Simulation and quantitative clarification of ac susceptibility of magnetic fluid in nonlinear Brownian relaxation region, Jpn. J. Appl. Phys. 45 (2009) 127002.
[9] M. Schilling, F. Ludwig, C. Kuhlmann, T. Wawrzik, Magnetic particle imaging scanner with 10 kHz drive-field frequency, Biomed. Tech 58 (6) (2013).
[10] T. Wawrzik, C. Kuhlmann, F. Ludwig, M. Schilling, Scanner setup and reconstruction for three-dimensional magnetic particle imaging, SPIE Med. Imaging 25 (2) (2013).
[11] J. Rahmer, J. Weizenecker, B. Gleich, J. Borgert, Signal encoding in magnetic particle imaging: properties of the system function, BMC Med. Imaging 9 (2009) 4.
[12] T. Wawrzik, T. Yoshida, M. Schilling, F. Ludwig, Debye-based frequency-domain magnetization model for magnetic nanoparticles in magnetic particle spectroscopy, IEEE Trans. Magn. 51 (2015) 2.
[13] J. Rahmer, A. Halkola, B. Gleich, I. Schmale, J. Borgert, First experimental evidence of the feasibility of multi-color magnetic particle imaging, Phys. Med. Biol. 60 (5) (2015).